Journal of Scientific Computing (2021) 88:16
https://doi.org/10.1007/s10915-021-01536-6

An Optimal Multigrid Algorithm for the Combining P_1-Q_1 Finite Element Approximations of Interface Problems Based on Local Anisotropic Fitting Meshes

Jun Hu[1] · **Hua Wang**[1]

Received: 2 November 2020 / Revised: 20 April 2021 / Accepted: 24 May 2021 / Published online: 1 June 2021

Abstract
A new finite element method is proposed for second order elliptic interface problems based on a local anisotropic fitting mixed mesh. The local anisotropic fitting mixed mesh is generated from an interface-unfitted mesh by simply connecting the intersected points of the interface and the underlying mesh successively. Optimal approximation capabilities on anisotropic elements are proved, the convergence rates are linear and quadratic in H^1 and L^2 norms, respectively. The discrete system is usually ill-conditioned due to anisotropic and small elements near the interface. Thereupon, a new multigrid method is presented to handle this issue. The convergence rate of the multigrid method is shown to be optimal with respect to both the coefficient jump ratio and mesh size. Numerical experiments are presented to demonstrate the theoretical results.

Keywords Interface-fitted mesh · Anisotropic element · Multigrid method

1 Introduction

Let Ω be a convex polygon in $\mathbb{R}^2$ which is separated by a C^2-continuous interface Γ into two sub-domains Ω_1 and Ω_2, see Figure 1 for an illustration. Consider the following interface problem

In this research, Jun Hu was supported by NSFC projects 11625101 and 11421101; Hua Wang was supported by China Postdoctoral Science Foundation Grand 2019M660277 and Jiangsu Key Lab for NSLSCS Grant 201906.

✉ Hua Wang
wanghua.math@foxmail.com

Jun Hu
hujun@math.pku.edu.cn

[1] School of Mathematical Sciences, Peking University, Beijing, China

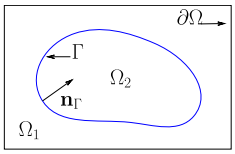

Fig. 1 A sketch of the domain for the interface problem

$$\begin{aligned} -\mathrm{div}(\beta\nabla u) &= f \quad \text{in } \Omega_1 \cup \Omega_2, \\ [\![u]\!] &= q \quad \text{on } \Gamma, \\ [\![\beta \frac{\partial u}{\partial \boldsymbol{n}_\Gamma}]\!] &= g \quad \text{on } \Gamma, \\ u &= 0 \quad \text{on } \partial\Omega, \end{aligned} \tag{1.1}$$

where $[\![v]\!] := (v|_{\Omega_1})|_\Gamma - (v|_{\Omega_2})|_\Gamma$ for any v belonging to $H^1(\Omega_1 \cup \Omega_2)$, and $\boldsymbol{n}_\Gamma$ is the unit normal vector of Γ which points from Ω_1 to Ω_2, see Figure 1. The coefficient function β is discontinuous across the interface Γ, i.e.,

$$\beta = \begin{cases} \beta_1, & \text{in } \Omega_1, \\ \beta_2, & \text{in } \Omega_2, \end{cases} \tag{1.2}$$

where β_1 and β_2 are positive constants.

This problem occurs widely in practical applications, such as fluid mechanics [17,24], electromagnetic wave propagations [30], materials sciences [23], and biological sciences [12]. Mathematically, the interface problem usually leads to partial differential equations with discontinuous or non-smooth solutions across interfaces. Hence, classical numerical methods designed for smooth solutions do not work efficiently. For regularity of the interface problem (1.1), Chen and Zou [11] proved that

$$\|u\|_{H^2(\Omega_1)} + \|u\|_{H^2(\Omega_2)} \le C_\beta(\|f\|_{L^2(\Omega)} + \|g\|_{H^{1/2}(\Gamma)}),$$

where C_β is a constant independent of u, f and g, but depends strongly and implicitly on the constants β_1, β_2 and the jump in the coefficient across the interface. Later, Huang and Zou [18,19] improved the estimate

$$|\beta_1 u|_{H^2(\Omega_1)} + |\beta_2 u|_{H^2(\Omega_2)} \le C(\|f\|_{L^2(\Omega)} + \|g\|_{H^{1/2}(\Gamma)}). \tag{1.3}$$

For more than four decades, there has been a growing interest in the interface problem, and a vast of literature is available, see [3,4,6,8,11,13,14,16,20–22,25,26,31]. There are two major classes of finite element methods (FEM) for the interface problem, namely, the interface-fitted FEMs and the interface-unfitted FEMs, categorized according to the topological relation between discrete grids and the interface. Accuracy would be lost if standard finite element methods are used on interface-unfitted meshes. One way to recover the approximate accuracy is to use interface-fitted meshes, such as [11,26]. Another way is to modify finite element spaces near the interface, see [15,21,31]. Interface-fitted mesh generation algorithms which can produce a semi-structured interface-fitted mesh in two and three dimensions are proposed by Chen et al. [9], and virtual element methods are applied to solve the elliptic interface problem. In [27], the authors proposed linear element schemes for diffusion equations and the Stokes equation with discontinuous coefficients on an interface-fitted grid which satisfies the maximal angle condition.

需要阅读这些文章

This work focuses on the interface-fitted mesh approach. Let $\mathcal{U}_h$ be a general quasi-uniform interface-unfitted mesh of Ω, an interface-fitted mesh $\mathcal{F}_h$ can be generated by simply connecting the intersected points of Γ and the mesh $\mathcal{U}_h$ successively. By this way, an interface-fitted

mesh can be generated quite efficiently no matter how complicated the interface is. It is obvious that the interface-fitted mesh $\mathcal{F}_h$ contains some anisotropic triangles and quadrilaterals near the interface. In [10,27], sub-quadrilaterals cut by Γ are further split and the generated grid is maximal-angle-bounded. Actually, it is not necessary to split these anisotropic sub-quadrilaterals. By using the approximation results for anisotropic quadrilaterals elements proposed by Acosta and Duran [1], optimal approximation capability of finite element spaces have been proved.

Since anisotropic elements and coefficient jump ratio may stiffen the matrix, a new multigrid method is presented for solving the discrete system. By coarsening the fitted mesh near the interface adaptively, a new multigrid V-cycle method is developed. It is shown that the convergence rate of this multigrid method is shown to be optimal with respect to the jump ratio and mesh size. In [25,27], the authors also studied multigrid methods for interface problems. Both of them can prove that the multigrid methods converge uniformly with respect to the mesh size, but not to the jump coefficients. However, the condition number of the stiff matrix highly depends on jump coefficients, our method is more suitable for interface problems with high-contrast coefficients. By assuming that each subdomain is an open disjointed polygonal, Xu and Zhu [28] proved the convergence rate of multigrid methods is uniform with respect to the large jump and mesh size. While, in this paper, the interface Γ is only assumed to be a general C^2-continuous curve.

The rest of this paper is organized as follows. In Section 2, we introduce some notations which will be frequently used in this paper. In Section 3, we present the local anisotropic finite element space and the weak form for the non-homogeneous second order elliptic interface problem. In Section 4, we derive an a prior estimate for the finite element method based on local anisotropic fitting mixed meshes. In Section 5, we propose a multigrid solver for the resulting linear system. We also present some numerical examples in Section 6 to validate our theoretical results.

2 Notation and Definitions

For integer $r \geq 0$, define the piecewise H^r Sobolev space

$$H^r(\Omega_1 \cup \Omega_2) = \{v \in L^2(\Omega); v|_{\Omega_i} \in H^r(\Omega_i), i = 1, 2\},$$

equipped with the norm and semi-norm

$$\|v\|_{H^r(\Omega_1 \cup \Omega_2)} = (\|v\|^2_{H^r(\Omega_1)} + \|v\|^2_{H^r(\Omega_2)})^{1/2},$$
$$|v|_{H^r(\Omega_1 \cup \Omega_2)} = (|v|^2_{H^r(\Omega_1)} + |v|^2_{H^r(\Omega_2)})^{1/2}.$$

Furthermore, let $\tilde{H}^r(\Omega_1 \cup \Omega_2) = H_0^1(\Omega) \cap H^r(\Omega_1 \cup \Omega_2)$.

In the following, a simple and efficient method is presented for generating interface-fitted mesh. Figures 2-3 show how to obtain an interface-fitted grid. The domain is a square and the interface is a circle. $\mathcal{U}_h$ is an quasi uniform mesh which does not fit to the interface. By connecting intersected points of Γ and $\mathcal{U}_h$ successively, a resolution Γ_h (the red line) of Γ (the blue line) is obtained. The generated mesh $\mathcal{F}_h$ is an interface-fitted mesh which contains anisotropic triangles and quadrilaterals near the interface.

Let $\Omega_{2,h}$ be an approximation of Ω_2, and $\Omega_{1,h}$ stand for the domain with $\partial\Omega$ and Γ_h as its exterior and interior boundaries, respectively (see Figure 3). Then, the domain Ω is separated into two sub-domains $\Omega_{1,h}$ and $\Omega_{2,h}$. The collection of interface elements in $\mathcal{U}_h$ and $\mathcal{F}_h$ is

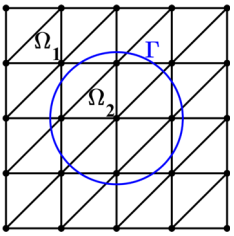

Fig. 2 An interface-unfitted mesh $\mathcal{U}_h$

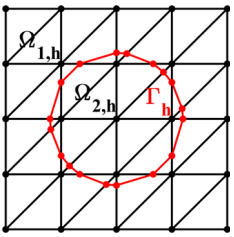

Fig. 3 An interface-fitted mesh $\mathcal{F}_h$

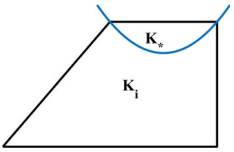

Fig. 4 A quadrilateral interface element in $\mathcal{F}_h$

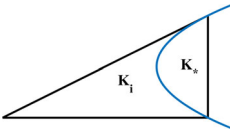

Fig. 5 A triangle interface element in $\mathcal{F}_h$

defined as

T的含义是任意单元，不是三角形这里?

$$\mathcal{U}_h^I = \{T \in \mathcal{U}_h; meas_1(T \cap \Gamma) > 0\},$$
$$\mathcal{F}_h^I = \{T \in \mathcal{F}_h; meas_1(T \cap \Gamma) > 0\},$$

where $meas_d$ denotes the d-dimensional measure. For any interface element $K \subset \Omega_{i,h}$, let $K_i = K \cap \Omega_i$ and $K_* = K \setminus K_i$, see Figures 4-5.

Let Ω_h^I be the region enclosed by Γ and Γ_h, i.e., $\Omega_h^I = (\Omega_{1,h} \setminus \Omega_1) \cup (\Omega_1 \setminus \Omega_{1,h})$. For any function $v \in H^2(\Omega_1 \cup \Omega_2)$, let $v_i = v|_{\Omega_i}$, $i = 1, 2$. By the extension theorem, if Γ is

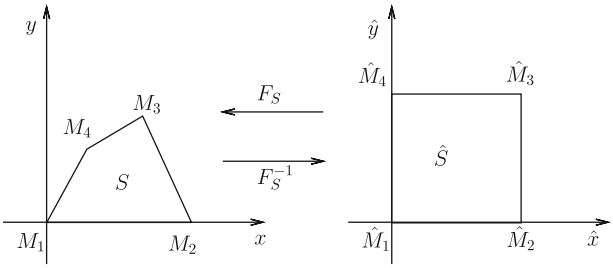

Fig. 6 A transformation from $\hat{S}$ to S

C^2-continuous, there exists an operator $E : H^2(\Omega_i) \to H^2(\Omega)$ such that

$$Ev_i|_{\Omega_i} = v_i, \quad \|Ev_i\|_{H^2(\Omega)} \lesssim \|v_i\|_{H^2(\Omega_i)}, \tag{2.1}$$

这里的延拓没有网格的概念?

for $i = 1, 2$ (see [2] for details). Here the notation $A \lesssim B$ represents the statement $A \leq$ constant $\times B$, where the constant is always independent of the mesh sizes of the triangulations and the location of the interface intersected with the mesh.

In order to analyze the interpolation error for these anisotropic triangles and quadrilaterals, the following are some basic definitions which mainly follow [5] and [1]. For the sake of convenience, we shall use S to represent a quadrilateral element, T for a triangle element, and K for a general element.

Definition 2.1 (Minimum angle condition) We say that a quadrilateral S (resp., a triangle T) satisfies $Minac(\alpha)$, if the angles of S (resp., T) are greater than or equal to α. Similarly, we say that a mesh $\mathcal{F}_h$ satisfies $Minac(\alpha)$, if there exists a uniform $\alpha \in (0, \pi]$ such that any $K \in \mathcal{F}_h$ satisfies $Minac(\alpha)$.

Definition 2.2 (Maximum angle condition) We say that a quadrilateral S (resp., a triangle T) satisfies $Maxac(\psi)$, if the angles of S (resp., T) are less than or equal to ψ. Similarly, we say that a mesh $\mathcal{F}_h$ satisfies $Maxac(\alpha)$, if there exists a uniform $\alpha \in (0, \pi]$ such that any $K \in \mathcal{F}_h$ satisfies $Maxac(\alpha)$.

Definition 2.3 Let S be a convex quadrilateral. We say that S satisfies the regular decomposition property with constants $N \in R$ and $0 < \psi < \pi$, or shortly $RDP(N, \psi)$, if we can divide S into two triangles along one of its diagonals, which will always be called d_1, in such a way that $|d_2|/|d_1| \leq N$ and both triangles satisfy $Maxac(\psi)$.

3 Finite Element Methods for the Elliptic Interface Problem

3.1 Finite Element Space

For a general convex quadrilateral S, denote its vertices by M_i in anticlockwise order. Let $\hat{S}$ be the reference unit square, $F_S : \hat{S} \to S$ be the transformation defined by

$$F_S(\hat{\mathbf{x}}) = \sum_{i=1}^{4} M_i \hat{\phi}_i(\hat{\mathbf{x}}), \tag{3.1}$$

where $\hat{\phi}_1 = (1 - \hat{x})(1 - \hat{y})$, $\hat{\phi}_2 = \hat{x}(1 - \hat{y})$, $\hat{\phi}_3 = \hat{x}\hat{y}$, $\hat{\phi}_4 = (1 - \hat{x})\hat{y}$. Observe that, F_S is a bijection from the unit square $\hat{S}$ onto the quadrilateral S.

The basis functions on S, no longer bilinears in general, are defined by $\phi_i(x) = \hat{\phi}_i(F_S^{-1}(x))$. Thus, the shape function space on S is defined by

$$\mathcal{Q}_1(S) = span\{\phi_i, 1 \leq i \leq 4\}.$$

Similarly, denote the linear shape function space on a general triangle T by $\mathcal{P}_1(T)$, i.e.,

$$\mathcal{P}_1(T) = span\{1, x, y\}.$$

Thus the finite element space defined on $\mathcal{F}_h$ can be written as

$$V_h = \{v_h \in C_0(\Omega); v_h|_T \in \mathcal{P}_1(T), v_h|_S \in \mathcal{Q}_1(S) \ \forall T, S \in \mathcal{F}_h\}. \tag{3.2}$$

只要求节点自由度相等并不能保证此条件? 由于四边形单元限制在某条边不一定是线性?

3.2 Weak Form

By the extension theorem, for any $q \in H^{3/2}(\Gamma)$, there exists a function $z_0 \in H^2(\Omega_2)$ s.t.

$$z_0|_\Gamma = -q, \quad \|z_0\|_{2,\Omega_2} \lesssim \|q\|_{3/2,\Gamma}.$$

Let

$$z = \begin{cases} 0, & \text{in } \Omega_1, \\ z_0, & \text{in } \Omega_2, \end{cases}$$

the non-homogeneous problem (1.1) can be rewritten as

$$\begin{aligned} -\mathrm{div}(\beta\nabla\tilde{u}) &= f + \mathrm{div}(\beta\nabla z) && \text{in } \Omega_1 \cup \Omega_2, \\ [\![\tilde{u}]\!] &= 0 && \text{on } \Gamma, \\ [\![\beta\frac{\partial\tilde{u}}{\partial n}]\!] &= g - [\![\beta\frac{\partial z}{\partial n}]\!] && \text{on } \Gamma, \\ \tilde{u} &= 0 && \text{on } \partial\Omega, \end{aligned} \tag{3.3}$$

with $\tilde{u} = u - z$. The variational formulation for the homogeneous problem (3.3) is: find $\tilde{u} \in V := H_0^1(\Omega)$ such that

$$a(\tilde{u}, v) = \tilde{F}(v) \quad \forall v \in V, \tag{3.4}$$

where

$$\begin{aligned} a(\tilde{u}, v) &= \int_{\Omega_1\cup\Omega_2} \beta\nabla\tilde{u} \cdot \nabla v dx, \\ \tilde{F}(v) &= \int_\Omega f v dx + \int_\Gamma g v ds - \int_{\Omega_2} \beta_2 \nabla z \cdot \nabla v dx. \end{aligned}$$

Let $\pi_h : C_0(\Omega) \mapsto V_h$ be the nodal interpolation operator, i.e.,

$$\pi_h u \in V_h, \quad \pi_h u(M) = u(M) \; \forall M \in \mathcal{O}, \tag{3.5}$$

where $\mathcal{O}$ is the set of nodal points of $\mathcal{F}_h$. Denote $\{O_i\}_{i=1}^m \subset \mathcal{O}$ the set of all nodes of the triangulation $\mathcal{F}_h$ lying on the interface Γ (the red points in Fig. 3), and $\{\phi_i\}_{i=1}^m$ the set of nodal basis functions associated to $\{O_i\}_{i=1}^m$. Assume g and q belong to $C(\Gamma)$, define

$$g_h = \sum_{i=1}^m g(O_i)\phi_i, \tag{3.6}$$

$$z_h|_{\Omega_{2,h}} = \pi_h z, \quad z_h|_{\Omega_{1,h}} = 0. \tag{3.7}$$

Usually, the integrals over Ω_i, and Γ could be performed exactly. A reasonable discrete weak form for the interface problem (3.3) with variational crimes is: find $\tilde{u}_h \in V_h$ such that

$$a_h(\tilde{u}_h, v_h) = \tilde{F}_h(v_h) \quad \forall v_h \in V_h, \tag{3.8}$$

where

$$a_h(\tilde{u}_h, v_h) = \int_{\Omega_{1,h}} \beta_1 \nabla \tilde{u}_h \cdot \nabla v_h dx + \int_{\Omega_{2,h}} \beta_2 \nabla \tilde{u}_h \cdot \nabla v_h dx$$
$$\tilde{F}_h(v_h) = \int_{\Omega} f v_h dx + \int_{\Gamma_h} g_h v_h ds - \int_{\Omega_{2,h}} \beta_2 \nabla z_h \cdot \nabla v_h dx.$$

Let $u_h = \tilde{u}_h + z_h$, it is obvious that u_h is an suitable approximation of u. However, z is a unknown function, therefore z_h is unknown either. Divide z_h into two parts

$$z_h = z_{h,\Gamma} + z_{h,0},$$

where

$$z_{h,\Gamma}|_{\Omega_{2,h}} = -\sum_{i=1}^{m} q(O_i)\phi_i, \quad z_{h,\Gamma}|_{\Omega_{1,h}} = 0.$$

Therefore, the discrete weak formulation (3.8) can be rewritten as: find $\bar{u}_h \in V_h$ such that

$$a_h(\bar{u}_h, v_h) = \bar{F}_h(v_h) \quad \forall v_h \in V_h, \tag{3.9}$$

where

$$\bar{F}_h(v_h) = \int_{\Omega} f v_h dx + \int_{\Gamma_h} g v_h ds - \int_{\Omega_{2,h}} \beta_2 \nabla z_{h,\Gamma} \cdot \nabla v_h dx.$$

Lemma 3.1 *Let $\tilde{u}_h$ and $\bar{u}_h$ be the solutions of Problem (3.8) and (3.9), respectively. The following relation holds*

$$u_h = \tilde{u}_h + z_h = \bar{u}_h + z_{h,\Gamma} \tag{3.10}$$

Proof Subtracting (3.9) from (3.8) yields that

$$a_h((\tilde{u}_h + z_{h,0}) - \bar{u}_h, v_h) = 0, \quad \forall v_h \in V_h.$$

Since $z_{h,0} \in V_h$, it is straightforward to see that

$$\tilde{u}_h + z_{h,0} = \bar{u}_h,$$

and consequently (3.10) holds. □

4 Error Analysis

4.1 Interpolation Error Estimates

Interpolation estimates are fundamental in finite element error analysis. Since the interpolation estimates on non-interface elements are standard, one only needs to consider the anisotropic elements near the interface.

Lemma 4.1 *([5], Theorem 2.3) Let T be a triangle with diameter h, if $v \in H^2(T)$, there exists a constant C independent of T such that*

$$\|v - \pi_h v\|_{L^2(T)} \leq Ch^2 |v|_{H^2(T)}, \tag{4.1}$$

and, if T satisfies $Maxac(\psi)$, then there exists a constant $C(\psi)$ which only depends on ψ such that

$$|v - \pi_h v|_{H^1(T)} \leq C(\psi) h |v|_{H^2(T)}. \tag{4.2}$$

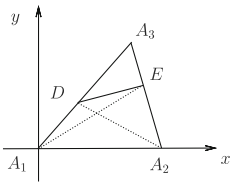

Fig. 7 An interface element in $\mathcal{U}_h^I$

Lemma 4.2 *([1], Theorem 4.7) Let S be a convex quadrilateral with diameter h, if $v \in H^2(S)$, there exists a constant C independent of S such that*

$$\|v - \pi_h v\|_{L^2(S)} \leq Ch^2 |v|_{H^2(S)}, \tag{4.3}$$

and, if S satisfies $RDP(N, \psi)$, then there exists a constant $C(N, \psi)$ which depends on N and ψ such that

$$|v - \pi_h v|_{H^1(S)} \leq C(N, \psi) h |v|_{H^2(S)}. \tag{4.4}$$

Lemma 4.3 *If $\mathcal{U}_h$ satisfies $Minac(\alpha)$, then for an arbitrary interface element $T := \triangle A_1A_2A_3 \in \mathcal{U}_h^I$ (see Figure 7),the triangle $\triangle A_3DE$ satisfies $Maxac(\psi_\alpha)$ and the quadrilateral A_1A_2ED satisfies $RDP(N_\alpha, \psi_\alpha)$, where N_α and ψ_α depend only on α.*

Proof Without loss of generality, assume A_1 is the origin and line A_1A_2 lies on the x-axis. Let the coordinates at A_1, A_2, A_3, D, E be

$$(0, 0), (x_2, 0), (x_3, y_3), (x_D, y_D), (x_E, y_E),$$

respectively, and suppose $\frac{|A_3D|}{|A_3A_1|} \geq \frac{|A_3E|}{|A_3A_2|}$, see Figure 7 for an illustration. Divide quadrilateral A_1A_2DE into two triangles, $\triangle A_1A_2D$ and $\triangle A_2ED$. Since $\mathcal{U}_h$ satisfies $Minac(\alpha)$, it follows that $\alpha \leq \angle DA_1A_2 \leq \pi - \alpha$. Hence triangle $\triangle A_1A_2D$ satisfies $Maxac(\pi - \alpha)$. Since $\frac{|A_3D|}{|A_3A_1|} \geq \frac{|A_3E|}{|A_3A_2|}$, it follows that $\angle A_3ED \geq \angle A_3A_2A_1$. And consequently

$$\alpha \leq \angle A_1A_3A_2 < \angle DEA_2 = \pi - \angle A_3ED \leq \pi - \angle A_3A_2A_1 \leq \pi - \alpha,$$

thus triangle $\triangle A_2ED$ satisfies $Maxac(\pi - \alpha)$. Moreover,

$$h \sin\alpha \lesssim |A_1A_3| |\sin\angle A_1A_3A_2| \leq |A_1E| \leq \max\{|A_1A_2|, |A_1A_3|\} \lesssim h,$$
$$h \sin\alpha \lesssim |A_2A_3| |\sin\angle A_1A_3A_2| \leq |A_2D| \leq \max\{|A_1A_2|, |A_2A_3|\} \lesssim h.$$

Therefore, it is easy to derive that

$$\frac{|A_1E|}{|A_2D|} \leq \frac{C}{\sin\alpha}.$$

Let $\psi_\alpha = \pi - \alpha$ and $N_\alpha = \frac{C}{\sin\alpha}$, it completes the proof. □

Lemma 4.4 *Assume $\mathcal{U}_h$ is a quasi-uniform mesh which satisfies $Minac(\alpha)$, and $\mathcal{F}_h$ is the interface-fitted mesh generated from $\mathcal{U}_h$ as in Fig. 3. Then, for any triangle $T \in \mathcal{F}_h$,*

$$T \text{ satisfies } Maxac(\psi_\alpha),$$

and any quadrilateral $S \in \mathcal{F}_h$,

$$S \text{ satisfies } RDP(N_\alpha, \psi_\alpha).$$

Proof Combining Theorem 4.2 with Lemma 4.3 completes the proof. □

为什么需要这个定理

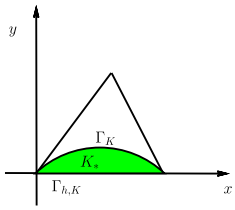

Fig. 8 A typical interface element in $\mathcal{F}_h$

Lemma 4.5 *Let K_* be the region enclosed by Γ_K and $\Gamma_{h,K}$, see Figure 8. For any $v \in H^1(K_*)$, it holds*

$$\|v\|_{L^2(K_*)} \lesssim h\|v\|_{L^2(\Gamma_K)} + h^2|v|_{H^1(K_*)}. \tag{4.5}$$

The proof included below was essentially due to Bramble and King [7].

Proof Assume that $\Gamma_{h,K}$ has its left endpoint at the origin and is given by

$$\Gamma_{h,K} = \{(x, y) \in K; 0 < x \leq \epsilon, y = 0\}.$$

Moreover, suppose that Γ_K can be denoted by

$$\Gamma_K = \{(x, y) \in K; 0 < x \leq \epsilon, y = \eta(x)\},$$

where $\epsilon(\lesssim h)$ is the length of $\Gamma_{h,K}$ and $\eta(x) \in C^2(0, \epsilon)$. Since the curvature of Γ is bounded, it is known that $\eta(x) \lesssim \epsilon^2$ and $\eta'(x) \lesssim \epsilon$. Let K_* be the region enclosed by Γ_K and $\Gamma_{h,K}$, by the divergence theorem

$$\int_{K_*} \nabla\cdot\boldsymbol{w}dxdy = \int_{\partial K_*} \boldsymbol{w}\cdot\boldsymbol{n}ds \quad \forall \boldsymbol{w} \in H(\mathrm{div}; K_*).$$

Let $\boldsymbol{w} = (0, yv^2)^K$ with $v \in H^1(K_*)$. Then,

$$\int_{K_*} v^2dxdy + \int_{K_*} 2yv\frac{\partial v}{\partial y}dxdy = \int_{\Gamma_K} yv^2(1 + (\eta'(x))^2)^{-1/2}ds.$$

Using the Cauchy-Schwarz inequality, it is easy to derive that

$$\begin{aligned}\|v\|^2_{0,K_*} &\leq C(\|y\|_{0,\infty,\Gamma_K}\|v\|^2_{0,\Gamma_K} + \|y\|_{0,\infty,\Gamma_K}\|v\|_{0,K_*}\|\frac{\partial v}{\partial y}\|_{0,K_*}) \\ &\leq C\epsilon^2\|v\|^2_{0,\Gamma_K} + C^2\epsilon^4\|\frac{\partial v}{\partial y}\|^2_{0,K_*} + \frac{1}{4}\|v\|^2_{0,K_*}.\end{aligned}$$

Therefore,

$$\|v\|_{0,T_*} \lesssim h\|v\|_{0,\Gamma_T} + h^2|v|_{1,T_*}.$$

□

The following theorem shows that the generated interface-fitted mesh does not reduce the approximation accuracy in spite of anisotropic elements.

Theorem 4.1 *For any $v \in \tilde{H}^2(\Omega_1 \cup \Omega_2)$, it holds that*

$$\|v - \pi_h v\|_{L^2(\Omega)} \lesssim h^2|v|_{H^2(\Omega_1\cup\Omega_2)}, \tag{4.6}$$

$$|v - \pi_h v|_{H^1(\Omega)} \lesssim h|v|_{H^2(\Omega_1\cup\Omega_2)}. \tag{4.7}$$

Proof For non-interface elements, the interpolation error estimate is standard. Assume $K \subset \Omega_{h,i}$ is a general (triangle or quadrilateral) interface element belonging to $\mathcal{F}_h^I$. According to Lemma 4.4, we know that K satisfies either $Maxac(\psi_\alpha)$ as a triangle or $RDP(N_\alpha, \psi_\alpha)$ as a quadrilateral. Then by Lemma 4.1 and Lemma 4.2, for any $w \in H^2(K)$,it holds that

$$\|w - \pi_h w\|_{L^2(K)} \lesssim h^2 |w|_{H^2(K)},$$
$$|w - \pi_h w|_{H^1(K)} \lesssim h |w|_{H^2(K)}.$$

Let E be the extension operator defined in Equation (2.1), it is easy to see that $\pi_h v = \pi_h E v_i$. For any $v \in \tilde{H}^2(\Omega_1 \cup \Omega_2)$, it follows that

$$\begin{aligned}
|v - \pi_h v|^2_{L^2(K)} &= |v_i - \pi_h v_i|^2_{L^2(K_i)} + |v_j - \pi_h v_i|^2_{L^2(K_*)} \\
&\lesssim |Ev_i - \pi_h E v_i|^2_{L^2(K)} + |v_j - Ev_i|^2_{L^2(K_*)} \\
&\lesssim h^4 |Ev_i|^2_{H^2(K)} + |v_j - Ev_i|^2_{L^2(K_*)} \qquad (\text{take} w = Ev_i) \\
&\lesssim h^4 |Ev_i|^2_{H^2(K)} + h^4 |v_j - Ev_i|^2_{H^1(K_*)} \quad (\text{by Lemma 4.5}) \\
&\lesssim h^4 (\|Ev_i\|^2_{H^2(K)} + \|v_j\|^2_{H^2(K_*)}),
\end{aligned}$$

where $i, j \in \{1, 2\}$ and $j \neq i$. Summing S over $\mathcal{F}_h^I$, it holds

$$\sum_{K \in \mathcal{F}_h^I} |v - \pi_h v|^2_{L^2(K)} \lesssim h^4 \|v\|^2_{H^2(\Omega_1 \cup \Omega_2)}.$$

Inequality (4.7) follows by using the same augment. □

4.2 An a Prior Error Estimate

In the following, the Galerkin approximation of (3.9) is analyzed in consideration of variational crimes. Recall the interface jump condition in the elliptic interface problem (1.1),

$$[\![u]\!] = q, \quad [\![\beta \frac{\partial u}{\partial n_\Gamma}]\!] = g \quad \text{on } \Gamma.$$

Lemma 4.6 *([11], Lemma 2.2) Assume $g \in H^2(\Gamma)$, it holds that*

$$|\int_\Gamma g v_h ds - \int_{\Gamma_h} g_h v_h ds| \lesssim h^{3/2} \|g\|_{H^2(\Gamma)} |v_h|_{H^1(\Omega_h^I)} \quad \forall v_h \in V_h. \tag{4.8}$$

If we don't use the approximation g_h for g in Problem (3.9), then $g \in H^{1/2}(\Gamma)$ is enough for the following error analysis.

Lemma 4.7 *Assume $q \in H^{3/2}(\Gamma)$, it holds that*

$$|z - z_h|_{H^1(\Omega_{2,h})} \lesssim h |z|_{H^2(\Omega_{2,h})}, \tag{4.9}$$
$$|\int_{\Omega_{2,h}} \beta_2 \nabla z_h \cdot \nabla v_h dx - \int_{\Omega_2} \beta_2 \nabla z \cdot \nabla v_h dx| \lesssim \beta_2 h \|u\|_{\tilde{H}^2(\Omega_1 \cup \Omega_2)} |v_h|_{H^1(\Omega_h^I)}. \tag{4.10}$$

Proof The estimate (4.9) is a direct consequence of Theorem 4.1. Using the triangle inequality, it follows that

$$|\int_{\Omega_{2,h}} \beta_2 \nabla z_h \cdot \nabla v_h dx - \int_{\Omega_2} \beta_2 \nabla z \cdot \nabla v_h dx|$$

$$
\begin{aligned}
&= |\int_{\Omega_{2,h}} \beta_2 \nabla(z_h - z)\cdot\nabla v_h dx + \int_{\Omega_{2,h}\setminus\Omega_2} \beta_2 \nabla z\cdot\nabla v_h dx - \int_{\Omega_2\setminus\Omega_{2,h}} \beta_2\nabla z\cdot\nabla v_h dx| \\
&\lesssim \beta_2(|z-z_h|_{H^1(\Omega_{2,h})} + |z|_{H^1(\Omega_h^I)})|v_h|_{H^1(\Omega_h^I)} \\
&\lesssim \beta_2 h|u|_{\tilde{H}^2(\Omega_1\cup\Omega_2)}|v_h|_{H^1(\Omega_h^I)}.
\end{aligned}
$$

□

Theorem 4.2 *Assume $u \in \tilde{H}^2(\Omega_1\cup\Omega_2)$ is the solution of Problem (1.1) and u_h is defined by (3.10), there exists a constant C_β depending on β such that*

$$|u-u_h|_{H^1(\Omega)} \le C_\beta h(\|f\|_{L^2(\Omega)} + \|g\|_{H^2(\Gamma)}), \tag{4.11}$$

$$\|u-u_h\|_{L^2(\Omega)} \le C_\beta h^2(\|f\|_{L^2(\Omega)} + \|g\|_{H^2(\Gamma)}). \tag{4.12}$$

Proof By using Lemma 3.1 and the triangle inequality, it yields that

$$
\begin{aligned}
|u-u_h|_{H^1(\Omega)} &= |\tilde{u}+z-\tilde{u}_h - z_h|_{H^1(\Omega)} \\
&\le |\tilde{u}-\tilde{u}_h|_{H^1(\Omega)} + |z-z_h|_{H^1(\Omega)}.
\end{aligned}
$$

The term $|z-z_h|_{H^1(\Omega)}$ is already analyzed in Lemma 4.7. By the standard analysis, it follows that

$$|\tilde{u}-\tilde{u}_h|_{H^1(\Omega)} \lesssim |\tilde{u}-\pi_h\tilde{u}|_{H^1(\Omega)} + \min\{\beta_1^{-1},\beta_2^{-1}\}\sup_{v_h\in V_h}\frac{a_h(\tilde{u}-\tilde{u}_h, v_h)}{|v_h|_{H^1(\Omega)}}.$$

The first term is the interpolation error proved in Theorem 4.1. The second term is the consistence error, and it is straightforward to show that

$$a_h(\tilde{u}-\tilde{u}_h, v_h) = (a_h(\tilde{u}, v_h) - a(\tilde{u}, v_h)) + (F(v_h) - \tilde{F}_h(v_h)).$$

The following sharpened embedding can be deduced from Lemma 4.5

$$\|v\|_{L^2(\Omega_h^I)} \lesssim h\|v\|_{H^1(\Omega_1\cup\Omega_2)} \qquad \forall v\in H^1(\Omega_1\cup\Omega_2). \tag{4.13}$$

By (4.13) and Lemma 4.6, it is easy to derive that

$$
\begin{aligned}
a_h(\tilde{u}, v_h) - a(\tilde{u}, v_h) &= \int_{\Omega_1\cap\Omega_{h,2}} (\beta_2-\beta_1)\nabla\tilde{u}\cdot\nabla v_h dx + \int_{\Omega_2\cap\Omega_{h,1}} (\beta_1-\beta_2)\nabla\tilde{u}\cdot\nabla v_h dx \\
&\lesssim |\beta_1-\beta_2||\tilde{u}|_{H^1(\Omega_h^I)}|v_h|_{H^1(\Omega)} \\
&\lesssim |\beta_1-\beta_2|h\|u\|_{\tilde{H}^2(\Omega_1\cup\Omega_2)}|v_h|_{H^1(\Omega)},
\end{aligned}
$$

and

$$
\begin{aligned}
F(v_h) - \tilde{F}_h(v_h) &= (\int_\Gamma g v_h ds - \int_\Gamma g_h v_h ds) + (\int_{\Omega_{2,h}} \beta_2\nabla z_h\cdot\nabla v_h dx \\
&\quad - \int_{\Omega_2}\beta_2\nabla z\cdot\nabla v_h dx) \\
&\lesssim h(\|g\|_{H^{3/2}(\Gamma)} + \beta_2\|u\|_{\tilde{H}^2(\Omega_1\cup\Omega_2)})|v_h|_{H^1(\Omega)}.
\end{aligned}
$$

The desired result (4.11) then follows by (1.3).

To show the L^2-norm error estimate (4.12), we use the Nitsche's trick. Consider the dual problem of Equation (3.4): find $w\in V$ such that

$$a(w, v) = (\tilde{u}-\tilde{u}_h, v) \qquad \forall v\in V, \tag{4.14}$$

and its finite element approximation: find $w_h\in V_h$ satisfying

$$a_h(w_h, v_h) = (\tilde{u} - \tilde{u}_h, v_h) \qquad \forall v_h \in V_h. \tag{4.15}$$

By the regularity result (1.3), it holds

$$\|w\|_{\tilde{H}^2(\Omega_1 \cup \Omega_2)} \leq C_\beta \|\tilde{u} - \tilde{u}_h\|_{L^2(\Omega)}. \tag{4.16}$$

Taking $v = \tilde{u} - \tilde{u}_h$ in (4.14), it yields that

$$\begin{aligned}
\|\tilde{u} - \tilde{u}_h\|^2_{L^2(\Omega)} &= (\tilde{u} - \tilde{u}_h, \tilde{u} - \tilde{u}_h) \\
&= a(w, \tilde{u} - \tilde{u}_h) \\
&= a(w - w_h, \tilde{u} - \tilde{u}_h) + a(w_h, \tilde{u} - \tilde{u}_h) \\
&= a(w - w_h, \tilde{u} - \tilde{u}_h) + (a_h(\tilde{u}_h, w_h) - a(\tilde{u}_h, w_h)) \\
&\quad + (a(\tilde{u}, w_h) - a_h(\tilde{u}_h, w_h)) \\
&\equiv: \text{(I)} + \text{(II)} + \text{(III)}.
\end{aligned}$$

The estimate (4.11) and (4.16) imply that

$$\begin{aligned}
\text{(I)} &\leq \max\{\beta_1, \beta_2\} |w - w_h|_{H^1(\Omega)} |\tilde{u} - \tilde{u}_h|_{H^1(\Omega)} \\
&\leq C_\beta h^2 \|w\|_{\tilde{H}^2(\Omega_1 \cup \Omega_2)} (\|f\|_{L^2(\Omega)} + \|g\|_{H^2(\Gamma)}) \\
&\leq C_\beta h^2 \|\tilde{u} - \tilde{u}_h\|_{L^2(\Omega)} (\|f\|_{L^2(\Omega)} + \|g\|_{H^2(\Gamma)}).
\end{aligned}$$

By the triangle inequality and (4.13), one can deduce that

$$\begin{aligned}
\text{(II)} &\leq |\beta_1 - \beta_2| |\tilde{u}_h|_{H^1(\Omega_h^I)} |w_h|_{H^1(\Omega_h^I)} \\
&\leq C_\beta (|\tilde{u}_h - \tilde{u}|_{H^1(\Omega_h^I)} + |\tilde{u}|_{H^1(\Omega_h^I)}) (|w_h - w|_{H^1(\Omega_h^I)} + |w|_{H^1(\Omega_h^I)}) \\
&\leq C_\beta h (\|\tilde{u}\|_{\tilde{H}^2(\Omega_1 \cup \Omega_2)} + \|g\|_{H^2(\Gamma)}) (h \|w\|_{\tilde{H}^2(\Omega_1 \cup \Omega_2)}) \\
&\leq C_\beta h^2 (\|f\|_{L^2(\Omega)} + \|g\|_{H^2(\Gamma)}) |\tilde{u} - \tilde{u}_h|_{L^2(\Omega)}.
\end{aligned}$$

Using Lemma 4.6 and Lemma 4.7, it holds

$$\begin{aligned}
\text{(III)} &= \tilde{F}(w_h) - \tilde{F}_h(w_h) \\
&\leq |\int_\Gamma g w_h ds - \int_{\Gamma_h} g_h w_h ds| + |\int_{\Omega_2} \beta_2 \nabla z \cdot \nabla w_h dx - \int_{\Omega_{2,h}} \beta_2 \nabla z_h \cdot \nabla w_h dx| \\
&\lesssim h^{3/2} \|g\|_{H^2(\Gamma)} |w_h|_{H^1(\Omega_h^I)} + \beta_2 h \|u\|_{\tilde{H}^2(\Omega_1 \cup \Omega_2)} |w_h|_{H^1(\Omega_h^I)} \\
&\leq C_\beta h (\|f\|_{L^2(\Omega)} + \|g\|_{H^2(\Gamma)}) (|w_h - w|_{H^1(\Omega_h^I)} + |w|_{H^1(\Omega_h^I)}) \\
&\leq C_\beta h^2 (\|f\|_{L^2(\Omega)} + \|g\|_{H^2(\Gamma)}) |\tilde{u} - \tilde{u}_h|_{L^2(\Omega_h^I)}.
\end{aligned}$$

Therefore, the L^2-error estimate follows from the estimations of the terms (I), (II) and (III). □

5 A Multi-grid Iterative Method

5.1 Spaces Decomposition

Suppose $\mathcal{U}_0$ is a quasi-uniform and regular triangulation of Ω with the mesh size h_0. Let $\mathcal{U}_l$, $1 \leq l \leq L$, be obtained from $\mathcal{U}_{l-1}$ via a "regular" subdivision: edge midpoints in $\mathcal{U}_{l-1}$ are connected by new edges to form $\mathcal{U}_l$.

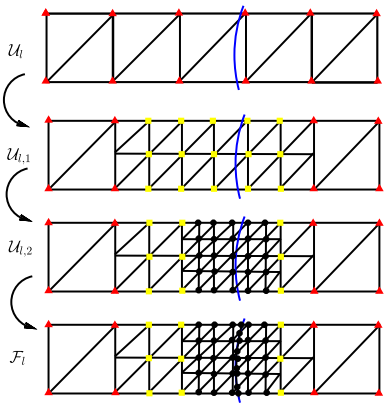

Fig. 9 An illustration for generating $\mathcal{F}_0$ with $L = 2$

For any integer $L \geq 2$, let $\mathcal{F}_L$ be an interface-fitted mesh generated from $\mathcal{U}_L$. In order to derive an optimal multi-grid method for the interface problem, we construct a sequence of nested triangulations $\{\mathcal{F}_l\}_{l=0}^{L}$ as follows, see Figure 9 for an illustration. The blue line is an interface, the red triangles, yellow squares and black points denotes degree of freedoms on different levels.

Algorithm 1 Generate an interface "adaptive" mesh $\mathcal{F}_l$ $(0 \leq l \leq L-1)$.

(1) Generate an interface-unfitted quasi-uniform mesh $\mathcal{U}_l$ with its mesh size equal h_l. Denote $\mathcal{U}_{l,0} = \mathcal{U}_l$;
(2) If $l < L$, refine $T \in \mathcal{U}_{l,j}$ via "regular" subdivision if T is an interface element or is a neighborhood of an interface element to get $\mathcal{U}_{l,j+1}$. Repeat step (2) to get $\mathcal{U}_{l,L-l}$;
(3) Connect intersected points of Γ and $\mathcal{U}_{l,L-l}$ to generate an interface-fitted grid $\mathcal{F}_l$;

Recall that $\mathcal{U}_l^I$ is the collection of interface elements in $\mathcal{U}_l$. Let $\mathcal{U}_{l,\Gamma}$ be an extension of $\mathcal{U}_l^I$ which also contains all neighbor elements of interface elements, i.e.,

$$\mathcal{U}_{l,\Gamma} = \{T \in \mathcal{U}_l; \exists \tilde{T} \in \mathcal{U}_l^I, s.t.\ \partial T \cap \partial \tilde{T} \neq \emptyset\}.$$

The corresponding region for the above element collection is denoted by $\Omega_{l,\Gamma}$ (The gray-painted area in Fig. 10). Define $\omega_{i,l} = \Omega_i \setminus \Omega_{l,\Gamma}$ for $i = 1, 2$. Consequently, the domain Ω admits the following division on the l-th level (see Figure 10)

$$\Omega = \bar{\Omega}_{l,\Gamma} \cup \omega_{l,1} \cup \omega_{l,2}. \tag{5.1}$$

Let $W_l = span\{\phi_{l,i}\}_{i=1}^{n_l}$ be the P_1 conforming finite element space defined on $\mathcal{U}_l$, where $\{\phi_{l,i}\}_{i=1}^{n_l}$ is the nature nodal basis such that $\phi_{l,i}(x_{l,j}) = \delta_{i,j}$ for each non-Dirichlet boundary node $x_{l,j}$. Decompose the space W_l according to the division of the domain Ω on $(l-1)$-th level

$$W_l = W_{l,\Gamma} \oplus W_{l,\omega},$$

where

$$W_{l,\Gamma} = span\{\phi_{l,i}; x_{l,i} \in \Omega_{l-1,\Gamma}\},$$
$$W_{l,\omega} = span\{\phi_{l,i}; x_{l,i} \in \Omega \setminus \Omega_{l-1,\Gamma}\}.$$

Define $n_{l,\Gamma} = \dim(W_{l,\Gamma})$ and $n_{l,\omega} = \dim(W_{l,\omega}) = n_l - n_{l,\Gamma}$. Without loss of generality, assume $W_{l,\omega} = span\{\phi_{l,i}\}_{i=1}^{n_{l,\omega}}$ and $W_{l,\Gamma} = span\{\phi_{l,i}\}_{i=n_{l,\omega}+1}^{n_l}$. Denote $\phi_{l,0} = \sum_{i=n_{l,\omega}+1}^{n_l} \phi_{l,i}$

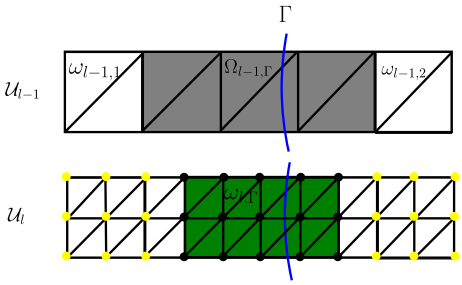

Fig. 10 An illustration for the space decomposition of W_l: black dots represent the degree of freedom of $W_{l,\Gamma}$; yellow dots represent the degree of freedom of $W_{l,\omega}$

and $\omega_{l,\Gamma} = \{(x, y) \in \Omega; \phi_{l,0}(x, y) \equiv 1\}$ (the green region in Fig. 10). In another word, $\omega_{l,\Gamma}$ is obtained by shrinking one element width inwards from $\Omega_{l-1,\Gamma}$.

Let V_L be the local anisotropic finite element space defined on $\mathcal{F}_L$ as in (3.2), and

$$V_{L,0} = \{v_h \in V_L; supp(v_h) \subset \Omega_{L-1,\Gamma}\}.$$

Then the coarse space $V_l (1 \le l \le L-1)$ associated with the interface adaptive mesh $\mathcal{F}_l$ is defined as follows

$$V_l = V_{l,0} \oplus V_{l,\omega}, \tag{5.2}$$

where

$$V_{l,0} = \sum_{j=l}^{L-1} W_{j,\Gamma} + V_{L,0},$$
$$V_{l,\omega} = W_{l,\omega},$$

and $V_0 = \sum_{j=0}^{L-1} W_{j,\Gamma} + V_{L,0}$. By the definition of V_l, the inclusion relation holds

$$V_0 \subset V_1 \subset \cdots \subset V_{L-1} \subset V_L.$$

For each space $V_{l,\omega}$, it can be further decomposed into micro pieces

$$V_{l,\omega} = \sum_{j=1}^{n_{l,\omega}} V_{l,j} = \sum_{j=1}^{n_{l,\omega}} span\{\phi_{l,j}\}.$$

Therefore, the decomposition of V_L can be written as follows

$$V_L = \sum_{l=0}^{L} V_l = V_0 + \sum_{l=1}^{L} (V_{l,0} + \sum_{j=1}^{n_{l,\omega}} V_{l,j}). \tag{5.3}$$

Remark 5.1 The key idea of the grid coarsening is to keep elements near the interface on each level without any coarsening, and coarsen elements far from the interface in a standard way. Since the number of degrees of freedom in elements near the interface $(V_{l,0})$ is $O(h_l^{-1})$, we can solve the residual equation on $V_{l,0}$ with an exact solver.

5.2 The Multigrid Algorithm

For convenience, let $a_L(\cdot,\cdot)$ be short for $a_{h_L}(\cdot,\cdot)$ and $\Omega_{i,L}$ be short for Ω_{i,h_L}, $i=1,2$. On each level $0 \le l \le L$, the operator $A_l : V_l \to V_l$ is defined by

$$(A_l v, w) = a_L(v, w) \quad \forall v, w \in V_l.$$

Then the weak formulation (3.9) is equivalent to the following operator equation

$$A_L u_L = F_L, \tag{5.4}$$

where $F_L \in V_L$ such that $(F_L, v) = \bar{F}_{h_L}(v), \forall v \in V_L$. For $v \in H^1(\Omega)$, define the following weighted L^2-norm and H^1-norm

$$\begin{aligned}
|||v|||_0 =& (\|\beta_1^{1/2} v\|^2_{L^2(\Omega_{1,L})} + \|\beta_2^{1/2} v\|^2_{L^2(\Omega_{2,L})})^{1/2},\\
|||v|||_1 =& (|\beta_1^{1/2} v|^2_{H^1(\Omega_{1,L})} + |\beta_2^{1/2} v|^2_{H^1(\Omega_{2,L})})^{1/2}.
\end{aligned}$$

And for any set $D \subset \Omega$, define

$$\begin{aligned}
|||v|||_{0,D} =& (\|\beta_1^{1/2} v\|^2_{L^2(\Omega_{1,L}\cap D)} + \|\beta_2^{1/2} v\|^2_{L^2(\Omega_{2,L}\cap D)})^{1/2},\\
|||v|||_{1,D} =& (|\beta_1^{1/2} v|^2_{H^1(\Omega_{1,L}\cap D)} + |\beta_2^{1/2} v|^2_{H^1(\Omega_{2,L}\cap D)})^{1/2}.
\end{aligned}$$

Let $Q_l : L^2(\Omega) \to V_l$ be the standard orthogonal L^2 projection defined by

$$(Q_l u, w) = (u, w) \ \ \forall w \in V_l.$$

For $j = 0, 1, \cdots, n_{l,\omega}$, define $P_{l,j} : V_L \to V_{l,j}$ by

$$a_L(P_{l,j} u, w) = a_L(u, w) \quad \forall w \in V_{l,j},$$

and $P_0 : V_L \to V_0$ is defined by

$$a_L(P_0 u, w) = a_L(u, w) \quad \forall w \in V_0.$$

Denoting $W_l(\Omega \setminus \Omega_{l-1,\Gamma}) = \{v|_{\Omega\setminus\Omega_{l-1,\Gamma}}; v \in W_l\}$, let $Q^{\omega}_{l,\beta} : L^2(\Omega \setminus \Omega_{l-1,\Gamma}) \to W_l(\Omega \setminus \Omega_{l-1,\Gamma})$ be the L^2 projection defined as follows

$$(\beta Q^{\omega}_{l,\beta} v, w)_{\Omega\setminus\Omega_{l-1,\Gamma}} = (\beta u, w)_{\Omega\setminus\Omega_{l-1,\Gamma}} \ \ \forall w \in W_l(\Omega \setminus \Omega_{l-1,\Gamma}).$$

Let $Q_{l,\beta} v \in W_l$ be such that

$$Q_{l,\beta} v = \begin{cases} 0, & \text{in } \omega_{l,\Gamma},\\ Q^{\omega}_{l,\beta} v, & \text{in } \Omega \setminus \Omega_{l-1,\Gamma}. \end{cases}$$

Since the region $\Omega_{l-1,\Gamma} \setminus \omega_{l,\Gamma}$ is a band of one triangular element width (see Figure 11), $Q_{l,\beta} v$ is a well-defined and unique function in W_l. By simultaneous approximation property, it holds

$$\left|\left|\left| v - Q_{l,\beta} v \right|\right|\right|_{0,\Omega\setminus\Omega_{l-1,\Gamma}} \lesssim h_l |||v|||_{1,\Omega\setminus\Omega_{l-1,\Gamma}}.$$

The block Gauss-Seidel smoother $R_l : V_l \to V_l$ is defined by

$$R_l = (I - \prod_{i=0}^{n_{l,\omega}} (I - P_{l,i})) A_l^{-1}.$$

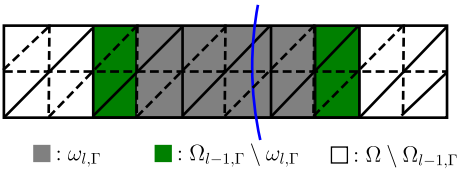

Fig. 11 An illustration for the definition of $Q_{l,\beta}$

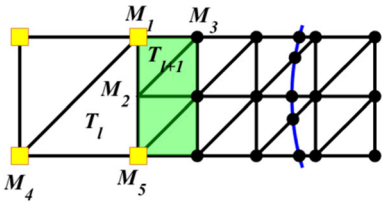

Fig. 12 The green-painted area: $\Omega_{l-1,\Gamma} \setminus \omega_{l,\Gamma}$

Remark 5.2 This block Gauss-Seidel smoother R_l means that

(1) do subspace correction on $V_{l,0}$ with an exact solver.
(2) do subspace correction on $V_{l,\omega}$ with the point Gauss-Seidle smoother.

The operator $B_L : V_L \to V_L$ is defined recursively as follows

Algorithm 2 (V-cycle)Let $B_0 = A_0^{-1}$, for $F_L \in V_L$, define $B_L F_L = u^{(3)}$.

(1)Presmoothing: $u^{(1)} = R_L F_L$;
(2)Correction: $u^{(2)} = u^{(1)} + B_{L-1} Q_{L-1}(F_L - A_L u^{(1)})$;
(3)Postsmoothing:$u^{(3)} = u^{(2)} + R_L^*(F_L - A_L u^{(2)})$;

It is straightforward to show that (see [29] for details)

$$I - B_L A_L = \left((I - P_0) \prod_{l=1}^{L} \prod_{i=0}^{n_{l,\omega}} (I - P_{l,i}) \right)^* \left((I - P_0) \prod_{l=1}^{L} \prod_{i=0}^{n_{l,\omega}} (I - P_{l,i}) \right). \tag{5.5}$$

5.3 V-cycle Convergence for the L^{th} Level Iteration

Let $\pi_l : C_0(\Omega) \to V_l$ be the nodal interpolation operator. Define $\Pi_l : V_L \to V_l$ by

$$\Pi_l v = Q_{l,\beta} v + \pi_l((\Pi_{l+1} v - Q_{l,\beta} v)\phi_{l,0}) \quad \text{for } l = L-1, L-2, \cdots, 0, \tag{5.6}$$

where $\Pi_L = I$. By the definition of $\phi_{l,0}$, it holds

$$\Pi_l v = \begin{cases} \Pi_{l+1} v, & \text{in } \omega_{l,\Gamma}, \\ Q_{l,\beta} v, & \text{in } \Omega \setminus \Omega_{l-1,\Gamma}. \end{cases} \tag{5.7}$$

Lemma 5.1 *For $0 \le l \le L-1$, it holds that*

$$|||(\Pi_{l+1} - \Pi_l)v|||_0 + h_l |||(\Pi_{l+1} - \Pi_l)v|||_1 \lesssim h_l |||v|||_1 \quad \forall v \in V_L. \tag{5.8}$$

Proof By the definition of Π_l, it has

$$(\Pi_{l+1} - \Pi_l)v = \begin{cases} 0, & \text{in } \omega_{l,\Gamma}, \\ (Q_{l+1,\beta} - Q_{l,\beta})v, & \text{in } \Omega \setminus \Omega_{l-1,\Gamma}. \end{cases}$$

Since

$$
\begin{aligned}
&\left|\!\left|\!\left|(Q_{l+1,\beta}-Q_{l,\beta})v\right|\!\right|\!\right|^2_{0,\Omega\setminus\Omega_{l-1,\Gamma}}+h_l^2\left|\!\left|\!\left|(Q_{l+1,\beta}-Q_{l,\beta})v\right|\!\right|\!\right|^2_{1,\Omega\setminus\Omega_{l-1,\Gamma}}\\
&\le\sum_{j=l}^{l+1}(\left|\!\left|\!\left|v-Q_{j,\beta}v\right|\!\right|\!\right|^2_{0,\Omega\setminus\Omega_{l-1,\Gamma}}+h_l^2\left|\!\left|\!\left|v-Q_{j,\beta}v\right|\!\right|\!\right|^2_{1,\Omega\setminus\Omega_{l-1,\Gamma}})\\
&\lesssim h_l^2|\!|\!|v|\!|\!|^2_1,
\end{aligned}
$$

it only needs to estimate $\left|\!\left|\!\left|(Q_{l+1,\beta}-Q_{l,\beta})v\right|\!\right|\!\right|_{0,\Omega_{l-1,\Gamma}\setminus\omega_{l,\Gamma}}$. Without loss of generality, assume $T_{l+1}\subset\Omega_{l-1,\Gamma}\setminus\omega_{l,\Gamma}$ as in Fig. 12. It is obvious that $T_{l+1}\subset\Omega\setminus\Omega_{l,\Gamma}$, therefore $\Pi_{l+1}v|_{T_{l+1}}=Q_{l+1,\beta}v$. A direct calculation shows that

$$
\begin{aligned}
|\!|\!|(\Pi_{l+1}-\Pi_l)v|\!|\!|^2_{0,T_{l+1}}&\lesssim h_{l+1}^2\sum_{1\le i\le 2}\beta(M_1)(Q_{l+1,\beta}v(M_i)-Q_{l,\beta}v(M_i))^2\\
&\lesssim h_{l+1}\beta(M_1)\|Q_{l+1,\beta}v-Q_{l,\beta}v\|^2_{0,M_1M_2}\\
&\lesssim h_{l+1}\beta(M_1)\|Q_{l+1,\beta}v-Q_{l,\beta}v\|^2_{0,M_1M_5}\\
&\lesssim \left|\!\left|\!\left|Q_{l+1,\beta}v-Q_{l,\beta}v\right|\!\right|\!\right|^2_{0,T_l}+h_{l+1}^2\left|\!\left|\!\left|Q_{l+1,\beta}v-Q_{l,\beta}v\right|\!\right|\!\right|^2_{0,T_l}\\
&\lesssim h_l^2|\!|\!|v|\!|\!|^2_{1,T_l}.
\end{aligned}
$$

Similarly, it is easy to derive that $|\!|\!|(\Pi_{l+1}-\Pi_l)v|\!|\!|^2_{1,T_{l+1}}\lesssim|\!|\!|v|\!|\!|^2_{1,T_l}$. Summing T_{l+1} over $\Omega_{l,\Gamma}\setminus\omega_{l,\Gamma}$, it yields

$$
|\!|\!|(\Pi_{l+1}-\Pi_l)v|\!|\!|^2_{0,\Omega_{l-1,\Gamma}\setminus\omega_{l,\Gamma}}+h_l^2|\!|\!|(\Pi_{l+1}-\Pi_l)v|\!|\!|^2_{1,\Omega_{l-1,\Gamma}\setminus\omega_{l,\Gamma}}\lesssim h_l^2|\!|\!|v|\!|\!|^2_1.
$$

This completes the proof. □

Lemma 5.2 *For $0\le l\le L$, it holds*

$$
|\!|\!|v-\Pi_l v|\!|\!|_0+h_l|\!|\!|v-\Pi_l v|\!|\!|_1\le Ch_l|\!|\!|v|\!|\!|_1\quad\forall v\in V_L. \tag{5.9}
$$

Proof By Lemma 5.1 and the triangle inequality, it's easy to derive that

$$
\begin{aligned}
&|\!|\!|v-\Pi_l v|\!|\!|_0+h_l|\!|\!|v-\Pi_l v|\!|\!|_1\\
&\le\sum_{r=l}^{L-1}(|\!|\!|\pi_{r+1}v-\Pi_r v|\!|\!|_0+h_r|\!|\!|\Pi_{r+1}v-\Pi_r v|\!|\!|_1)\\
&\lesssim h_l|\!|\!|v|\!|\!|_1.
\end{aligned}
$$

□

According to the space decomposition (5.3), for any $v\in V_L$, do the following decomposition

$$
v=v_0+\sum_{l=1}^{L}(v_{l,0}+\sum_{i=1}^{n_{l,\omega}}v_{l,i}), \tag{5.10}
$$

where $v_0=\Pi_0 v\in V_0$, and $v_{l,i}=\pi_l((\Pi_l v-\Pi_{l-1}v)\phi_{l,i})\in V_{l,i}$ for $i=0,1,\cdots,n_{l,\omega}$.

Theorem 5.1 *The V-cycle algorithm (2) has the following convergence rate estimate*

$$
\|I-B_LA_L\|_{A_L}\le 1-\frac{1}{1+C|\log h_L|}. \tag{5.11}
$$

The proof included below mainly follows [28], specific details are still given for completeness.

Proof By X-Z identity (see [29]), it holds

$$\|I - B_L A_L\|_{A_L} \leq 1 - \frac{1}{1+c_0},$$

with

$$c_0 = \sup_{|||v|||_1=1} \inf_{v=v_0+\sum_{l=1}^{L}\sum_{i=0}^{n_{l,\omega}} v_{l,i}} c(v),$$

where

$$c(v) = |||P_0(v-v_0)|||_1^2 + \sum_{l=1}^{L}\sum_{i=0}^{n_{l,\omega}} \left|\left|\left| P_{l,i} \sum_{(k,j)>(l,i)} v_{k,j} \right|\right|\right|_1^2.$$

Let $\Delta_{l,i} = supp(\phi_{l,i})$ and notice

$$\sum_{(k,j)>(l,i)} v_{k,j} = (v - \Pi_l v) + \sum_{j=i+1}^{n_{l,\omega}} v_{l,j},$$

$$\begin{aligned}\sum_{l=1}^{L}\sum_{i=0}^{n_{l,\omega}} \left|\left|\left| P_{l,i} \sum_{(k,j)>(l,i)} v_{k,j} \right|\right|\right|_1^2 &\lesssim \sum_{l=1}^{L}\sum_{i=0}^{n_{l,\omega}} \left(|||P_{l,i}(v-\Pi_l v)|||_1^2 + \left|\left|\left| P_{l,i} \sum_{j=i+1}^{n_{l,\omega}} v_{l,j} \right|\right|\right|_1^2 \right) \\ &\lesssim \sum_{l=1}^{L}\sum_{i=0}^{n_{l,\omega}} \left(|||v-\Pi_l v|||_{1,\Delta_{l,i}}^2 + \sum_{j=i+1}^{n_{l,\omega}} |||v_{l,j}|||_{1,\Delta_{l,i}}^2 \right) x.\end{aligned}$$

Observe that

$$\sum_{l=1}^{L}\sum_{i=0}^{n_{l,\omega}} |||v-\Pi_l v|||_{1,\Delta_{l,i}}^2 = \sum_{l=1}^{L} |||v-\Pi_l v|||_{1,\Omega}^2 \lesssim |\log h_L| |||v|||_{1,\Omega}^2,$$

and

$$\begin{aligned}\sum_{l=1}^{L}\sum_{i=0}^{n_{l,\omega}}\sum_{j=i+1}^{n_{l,\omega}} |||v_{l,j}|||_{1,\Delta_{l,i}}^2 &\lesssim \sum_{l=1}^{L} \left(|||v_{l,0}|||_{1,\Delta_{l,0}}^2 + \sum_{i=1}^{n_{l,\omega}}\sum_{j=i+1}^{n_{l,\omega}} h_l^{-2} |||v_{l,j}|||_{0,\Delta_{l,i}}^2 \right) \\ &\lesssim \sum_{l=1}^{L} \Big(|||\pi_l((\Pi_l v - \Pi_{l-1} v)\phi_{l,0})|||_{1,\Delta_{l,0}}^2 \\ &\quad + \sum_{i=1}^{n_{l,\omega}}\sum_{j=i+1}^{n_{l,\omega}} h_l^{-2} |||v_{l,j}|||_{0,\Delta_{l,i}}^2 \Big) \\ &\lesssim \sum_{l=1}^{L} \left(|||\Pi_l v - \Pi_{l-1} v|||_{1,\Delta_{l,0}}^2 + \sum_{i=0}^{n_{l,\omega}} h_l^{-2} |||\Pi_l v - \Pi_{l-1} v|||_{0,\Delta_{l,i}}^2 \right) \\ &\lesssim |\log h_L| |||v|||_1^2.\end{aligned}$$

Combining the above inequalities concludes the proof. □

Table 1 Finite element errors for **Example 1** with $\beta_1 = 10^4$, $\beta_2 = 1$

$\frac{1}{h}$	$\|u - u_h\|_{0,\Omega}$	order	$\|u - u_h\|_{1,\Omega}$	order
32	1.3399e-03		3.3520e-02	
64	3.6122e-04	1.8911	1.7466e-02	0.9404
128	9.0503e-05	1.9968	8.8375e-03	0.9828
256	2.2666e-05	1.9974	4.4497e-03	0.9899
512	5.6388e-06	2.0070	2.2724e-03	0.9694

Table 2 Finite element errors for **Example 1** with $\beta_1 = 10^2$, $\beta_2 = 1$

$\frac{1}{h}$	$\|u - u_h\|_{0,\Omega}$	order	$\|u - u_h\|_{1,\Omega}$	order
32	1.3415e-03		3.3523e-02	
64	3.6107e-04	1.8935	1.7467e-02	0.9404
128	9.0456e-05	1.9969	8.8399e-03	0.9825
256	2.2638e-05	1.9984	4.4511e-03	0.9898
512	5.6057e-06	2.0138	2.2727e-03	0.9697

6 Numerical Examples

In this section, we present several numerical examples to show the performance of our methods. Particular attention will be paid on verifying its high order convergence and examining its robustness in dealing with low regularity solutions and complex geometries. The computational domain is the rectangle $-1 \le x, y \le 1$, and the interface is denoted by a levelset function $\phi(x, y)$, i.e.,

$$\Omega = \{(x, y) \in \mathbb{R}^2; -1 \le x, y \le 1\},$$
$$\Omega_1 = \{(x, y) \in \Omega; \phi(x, y) > 0\},$$
$$\Omega_2 = \{(x, y) \in \Omega; \phi(x, y) < 0\}.$$

We test the multigrid algorithm 2 with these examples, the initial guess is $\mathbf{0}$, and the stopping criterion is the l^2 norm of the relative residual being smaller than exp(-20).

6.1 Example 1

The interface is a circle centered at the origin with radius r, i.e.,

$$\phi(x, y) = x^2 + y^2 - r^2.$$

The exact solution is chosen as follows

$$u = \frac{1}{\beta}\phi(x, y)\sin(\pi x)\sin(\pi y).$$

We test the local anisotropic FEM for the second order elliptic interface problem (1.1) whose exact solutions are defined as above and whose coefficient jump ratio $\beta_1/\beta_2 = 10^4, 10^2, 10^{-2}, 10^{-4}$. Numerical results are shown in Tables 1-4, illustrating that the convergence rates are optimal in H^1-norm and L^2-norm. Figure 13 illustrates that our method allows discontinuity of the gradient of the solution u on the interface.

Table 3 Finite element errors for **Example 1** with $\beta_1 = 1$, $\beta_2 = 10^2$

$\frac{1}{h}$	$\|u - u_h\|_{0,\Omega}$	order	$\|u - u_h\|_{1,\Omega}$	order
32	3.9442e-03		9.7003e-02	
64	9.9666e-04	1.9845	4.8823e-02	0.9904
128	2.5030e-04	1.9934	2.4450e-02	0.9977
256	6.2653e-05	1.9982	1.2252e-02	0.9967
512	1.5648e-05	2.0013	6.1377e-03	0.9973

Table 4 Finite element errors for **Example 1** with $\beta_1 = 1$, $\beta_2 = 10^4$

$\frac{1}{h}$	$\|u - u_h\|_{0,\Omega}$	order	$\|u - u_h\|_{1,\Omega}$	order
32	3.9444e-03		9.7007e-02	
64	9.9671e-04	1.9845	4.8825e-02	0.9904
128	2.5033e-04	1.9933	2.4450e-02	0.9977
256	6.2665e-05	1.9981	1.2253e-02	0.9967
512	1.5659e-05	2.0006	6.1379e-03	0.9973

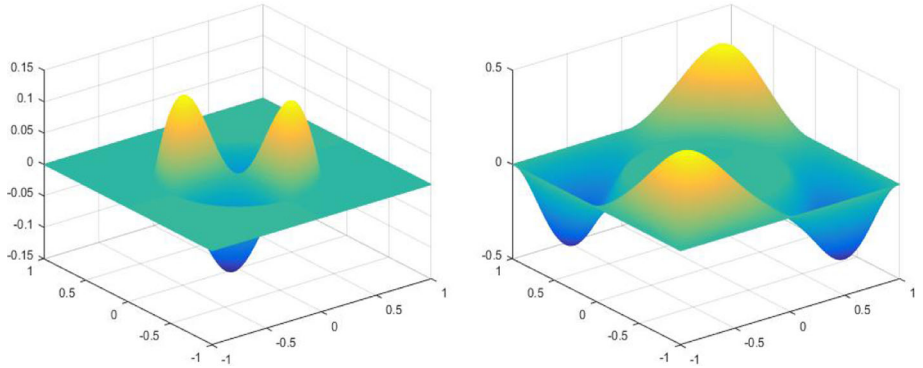

Fig. 13 Numerical solutions for **Example 1** with $\beta_1/\beta_2 = 10^4$(left) and $\beta_1/\beta_2 = 10^{-4}$(right)

Table 5 Numerical performance of Algorithm 2 for **Example 1** with $\beta_1/\beta_2 = 10^{-4}$

h	2^{-6}	2^{-7}	2^{-8}	2^{-9}
#iter	8	8	8	8

From Tables 5-6, we can see that the desired multigrid method converges uniformly with respect to the mesh size and the jump ratio.

Table 6 Numerical performance of Algorithm 2for **Example 1** with $h = 2^{-9}$

β_1/β_2	10^4	10^2	10^{-2}	10^{-4}
#iter	8	8	8	8

Fig. 14 A cardioid interface

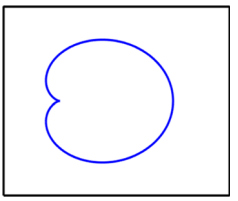

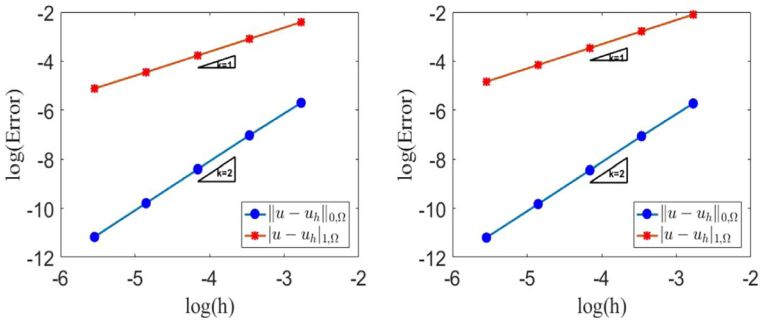

Fig. 15 Finite element error analysis in log-log scale for **Example 2** with $\beta_1/\beta_2 = 10^3$(left) and $\beta_1/\beta_2 = 10^{-3}$(right)

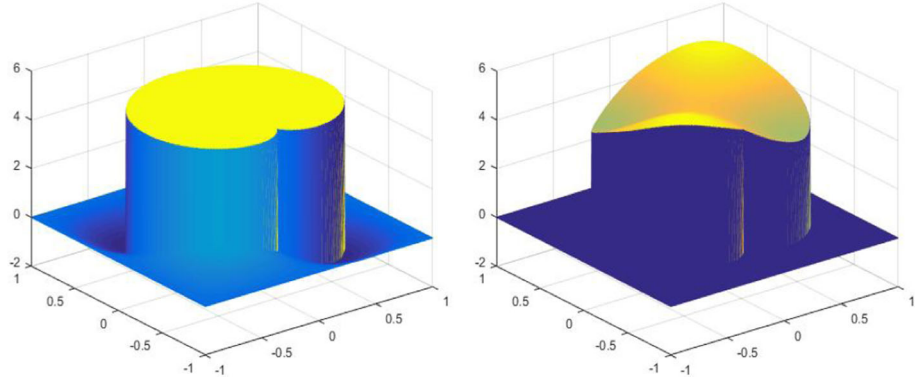

Fig. 16 Numerical solutions for **Example 2** with $\beta_1/\beta_2 = 10^3$(left) and $\beta_1/\beta_2 = 10^{-3}$(right)

Fig. 17 A five star and a circle interfaces

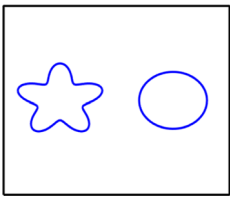

6.2 Example 2

The interface is a cardioid curve (see Figure 14),

$$\phi(x, y) = ((x + 0.5)^2 + y^2 - 0.5(x + 0.5))^2 - 0.25((x + 0.5)^2 + y^2).$$

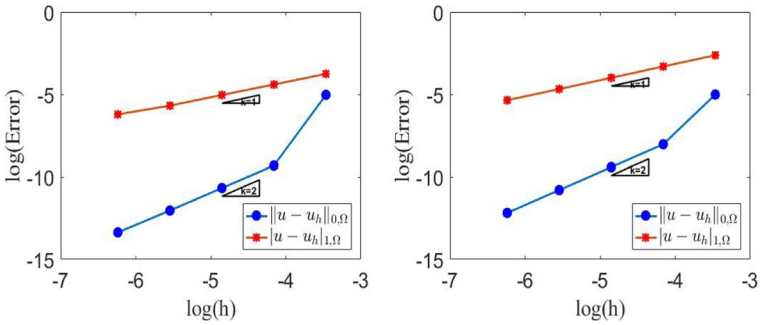

Fig. 18 Finite element error analysis in log-log scale for **Example 3** with $\beta_1/\beta_2 = 10^3$(left) and $\beta_1/\beta_2 = 10^{-3}$(right)

Table 7 Numerical performance of Algorithm 1 for **Example 2** with $\beta_1/\beta_2 = 10^{-4}$

h	2^{-6}	2^{-7}	2^{-8}	2^{-9}
#iter	9	9	9	9

Table 8 Numerical performance of Algorithm 2 for **Example 2** with $h = 2^{-9}$

β_1/β_2	10^4	10^2	10^{-2}	10^{-4}
#iter	9	9	9	9

Then the exact solution is chosen as follows

$$u = \frac{1}{\beta}\sin(\pi x)\sin(\pi y) + 5\delta(x, y),$$

where

$$\delta(x, y) = \begin{cases} 0, & (x, y) \in \Omega_1, \\ 1, & (x, y) \in \Omega_2. \end{cases}$$

We test our method for the second order elliptic interface problem (1.1) whose exact solutions are defined as above and whose coefficient jump ratio $\beta_1/\beta_2 = 10^3, 10^{-3}$, Numerical results are shown in Fig. 18, illustrating that the convergence rates are optimal in H^1-norm and L^2-norm. For the non-homogeneous case, Table 7-8 show that our multigrid algorithm is still optimal.

6.3 Example 3

There are two interfaces in this example, one is a five star curve, the other is a circle (see Figure 17), i.e,

$$\phi(x, y) = (\rho_1 - 0.3 - 0.09\sin(5\theta))(\rho_2^2 - 0.09),$$

where $\rho_1 = (x + 0.5)^2 + y^2$, $\rho_2 = (x - 0.5)^2 + y^2$. The exact solution is chosen as follows

$$u = \frac{1}{\beta}\sin(\pi x)\sin(\pi y) + \delta(x, y).$$

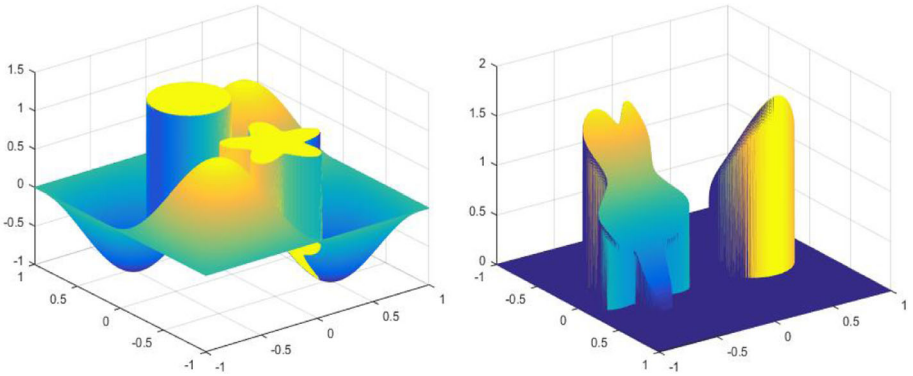

Fig. 19 Numerical solutions for **Example 3** with $\beta_1/\beta_2 = 10^3$(left) and $\beta_1/\beta_2 = 10^{-3}$(right)

Table 9 Numerical performance of Algorithm 2 for **Example 3** with $\beta_1/\beta_2 = 10^{-4}$

h	2^{-6}	2^{-7}	2^{-8}	2^{-9}
#iter	8	8	8	8

Table 10 Numerical performance of Algorithm 2 for **Example 3** with $h = 2^{-9}$

β_1/β_2	10^4	10^2	10^{-2}	10^{-4}
#iter	8	8	8	8

We test the local anisotropic FEM for the second order elliptic interface problem (1.1) whose exact solutions are defined as above and whose coefficient jump ratio $\beta_1/\beta_2 = 10^3, 10^{-3}$. Numerical results are shown in Fig. 18, illustrating that the convergence rates are optimal in H^1-norm and L^2-norm.

Still Table 7-8 show that our multigrid algorithm has an optimal convergence rate independent of the mesh size and jump ratio.

References

1. Acosta, G., Duran, R.G.: Error estimates for Q_1 isoparametric elements satisfying a weak angle condition. SIAM J. Num. Anal. **38**, 1073–1088 (2000)
2. Adams, R. A., Fournier, J. J.: *Sobolev Spaces*. Academic press, (2003)
3. Adjerid, S., Chaabane, N., Lin, T.: An immersed discontinuous finite element method for Stokes interface problems. Comput. Methods Appl. Mech. Eng. **293**, 170–190 (2015)
4. Babuška, I.: The finite element method for elliptic equations with discontinuous coefficients. Computing **5**, 207–213 (1970)
5. Babuška, I., Aziz, A.K.: On the angle condition in the finite element method. SIAM J. Num. Anal. **13**, 214–226 (1976)
6. Belytschko, T., Black, T.: Elastic crack growth in finite elements with minimal remeshing. Int. J. Num. Methods Eng. **45**, 601–620 (1999)
7. Bramble, J.H., King, J.T.: A finite element method for interface problems in domains with smooth boundaries and interfaces. Adv. Comput. Math. **6**, 109–138 (1996)
8. Burman, E., Guzmán, J., Sánchez, M.A., Sarkis, M.: Robust flux error estimation of an unfitted Nitsche method for high-contrast interface problems. IMA Journal of Numerical Analysis (2016)
9. Chen, L., Wei, H., Wen, M.: An interface-fitted mesh generator and virtual element methods for elliptic interface problems. J. Comput. Phys. **334**, 327–348 (2017)

10. Chen, Z., Wu, Z., Xiao, Y.: An adaptive immersed finite element method with arbitrary Lagrangian-Eulerian scheme for parabolic equations in time variable domains. Int. J. Num. Analy. Model. **12**, 567–591 (2015)
11. Chen, Z., Zou, J.: Finite element methods and their convergence for elliptic and parabolic interface problems. Numerische Mathematik **79**, 175–202 (1998)
12. Cumsille, P., Asenjoc, J., Conca, C.: A novel model for biofilm growth and its resolution by using the hybrid immersed interface-level set method. Comput. Math. Appl. **67**, 34–51 (2014)
13. Guzmán, J., Sánchez, M., Sarkis, M.: On the accuracy of finite element approximations to a class of interface problems. Math. Comput. **85**(301), 2071–2098 (2016)
14. Hansbo, A., Hansbo, P.: An unfitted finite element method, based on Nitsche's method, for elliptic interface problems. Comput. Methods Appl. Mech. Eng. **191**, 5537–5552 (2002)
15. Hansbo, A., Hansbo, P.: A finite element method for the simulation of strong and weak discontinuities in solid mechanics. Comput. Methods Appl. Mech. Eng. **193**, 3523–3540 (2004)
16. Hansbo, P., Larson, M.G., Zahedi, S.: A cut finite element method for a Stokes interface problem. Appl. Num. Math. **85**, 90–114 (2014)
17. Hou, T., Li, Z., Osher, S., Zhao, H.: A hybrid method for moving interface problems with application to the Hele-Shaw flow. J. Comput. Phys. **134**, 236–252 (1997)
18. Huang, J., Zou, J.: Some new a priori estimates for second order elliptic and parabolic interface problems. J. Diff. Equa. **184**, 570–586 (2002)
19. Huang, J., Zou, J.: Uniform a priori estimates for elliptic and static Maxwell interface problems. Dis. Contin. Dynam. Syst.-Series B **7**, 145–170 (2007)
20. Kergrene, K., Babuška, I., Banerjee, U.: Stable generalized finite element method and associated iterative schemes; application to interface problems. Comput. Methods Appl. Mech. Eng. **305**, 1–36 (2016)
21. Li, Z.: The immersed interface method using a finite element formulation. Appl. Num. Math. **27**, 253–267 (1998)
22. Li, Z., Lin, T., Wu, X.: New Cartesian grid methods for interface problems using the finite element formulation. Numerische Mathematik **96**, 61–98 (2003)
23. Ma, Q., Cui, J., Li, Z., Wang, Z.: Second-order asymptotic algorithm for heat conduction problems of periodic composite materials in curvilinear coordinates. J. Comput. Appl. Math. **306**, 85–115 (2016)
24. Sussman, M., Smereka, P., Osher, S.: A level set approach for computing solutions to incompressible two-phase flow. J. Comput. Phys. **114**, 146–159 (1994)
25. Xiao, Y., Xu, J., Wang, F.: High order eXtended finite element methods for interface problems. Comput. Methods Appl. Mech. Eng. **364**, 1–21 (2020)
26. Xu, J.: Estimate of the convergence rate of finite element solutions to elliptic equations of second order with discontinuous coefficients. Natl. Sci. J. Xiangtan Univ. (in Chinese) **1**, 84–88 (1982)
27. Xu, J., Zhang, S.: Optimal finite element methods for interface problems. *Domain Decomposition Methods in Science and Engineering XXII*, pages 77–91, (2016)
28. Xu, J., Zhu, Y.: Uniform convergent multigrid methods for elliptic problems with strongly discontinuous coefficients. Math. Model. Methods Appl. Sci. **18**, 77–105 (2008)
29. Xu, J., Zikatanov, L.: The method of alternating projections and the method of subspace corrections in Hilbert space. J. Am. Math. Soc. **15**, 573–597 (2002)
30. Zhang, Y., Nguyen, D., Du, K., Xu, J., Zhao, S.: Time-domain numerical solutions of Maxwell interface problems with discontinuous electromagnetic waves. Adv. Appl. Math. Mech. **8**, 353–385 (2016)
31. Zi, G., Belytschko, T.: New crack-tip elements for XFEM and applications to cohesive cracks. Int. J. Num. Methods Eng. **57**, 2221–2240 (2003)